Published in final edited form as:
J Neuropathol Exp Neurol. 2011 February ; 70(2): 157–165. doi:10.1097/NEN.0b013e31820937e4.

Reduced Axonopathy and Enhanced Remyelination Following Chronic Demyelination in Fibroblast Growth Factor-2 *(Fgf2)* Null Mice: Differential Detection with Diffusion Tensor Imaging

Jennifer E. Tobin, PhD[1,3,*], **Mingqiang Xie, PhD**[2,4,*], **Tuan Q. Le**[1], **Sheng-Kwei Song, PhD**[2], and **Regina C. Armstrong, PhD**[1]

[1] Department of Anatomy, Physiology and Genetics, Uniformed Services University of the Health Sciences, Bethesda, Maryland [2] Department of Radiology, Washington University School of Medicine, St. Louis, Missouri

Abstract

Chronic central nervous system demyelinating diseases result in long-term disability due to limited remyelination capacity and cumulative damage to axons. Corpus callosum demyelination in mice fed cuprizone provides a reproducible model of chronic demyelination in which the demyelinating agent can be removed to test modifications that promote recovery and to develop non-invasive neuroimaging techniques for monitoring changes in myelin and axons. We used the cuprizone model in mice with genetic deletion of *fibroblast growth factor-2* (*Fgf2*) to determine the impact of FGF2 on axon pathology and remyelination following chronic demyelination. We also evaluated the ability of quantitative magnetic resonance diffusion tensor imaging (DTI) to distinguish the corresponding pathological changes in axons and myelin during the progression of demyelination and remyelination. During the recovery period following chronic demyelination, *Fgf2* null mice exhibited enhanced remyelination that was detected using DTI measures of radial diffusivity and confirmed by electron microscopic analysis of the proportion of remyelinated axons. Ultrastructural analysis also demonstrated reduced axonal atrophy in chronically demyelinated *Fgf2* null vs. wild type mice. This difference in axon atrophy was further demonstrated as reduced immunohistochemical detection of neurofilament dephosphorylation in *Fgf2* null mice. DTI axial and radial diffusivity measures did not differentiate *Fgf2* null mice from wild type mice to correlate with changes in axonal atrophy during chronic demyelination. Overall, these findings demonstrate that attenuation of FGF2 signaling promotes neuroprotection of axons and remyelination, suggesting that FGF2 as an important negative regulator of recovery following chronic demyelination.

Keywords

Axon damage; Diffusion tensor imaging; Fibroblast growth factor; Oligodendrocyte progenitors; Regeneration; Remyelination

Correspondence and reprint requests to: Regina C. Armstrong, PhD, Department of Anatomy, Physiology and Genetics, Uniformed Services University of the Health Sciences, 4301 Jones Bridge Rd., Bethesda, MD 20814. Tel: (301) 295–3205; Fax: (301) 295–1715; rarmstrong@usuhs.edu.
[3]Science Applications International Corporation, 5202 President's Court, Suite 110, Frederick, Maryland.
[4]Department of Pathology & Immunology, Washington University School of Medicine, St. Louis, Missouri.
[*]Contributed equally.

INTRODUCTION

Multiple sclerosis (MS) is the most common human demyelinating disease and the main cause of non-traumatic neurological disability in young adults in North America and Europe (1). In MS, spontaneous remyelination of demyelinated lesions can be effective, especially early in the disease course. However, repeated or prolonged episodes of demyelination can stifle the capacity for repair as well as increase damage to axons. Multiple factors may contribute to poor repair of chronically demyelinated lesions, including depletion of oligodendrocyte progenitor (OP) cells and signals in the lesion environment that inhibit OP differentiation, such as fibroblast growth factor 2 (FGF2), Jagged-1, Lingo-1, and hyaluronic acid (2–5).

Interpreting the effects of FGF2 on the oligodendrocyte lineage during remyelination has been controversial. Contradictory findings have resulted from in vivo studies of FGF2 administration in CNS white matter. For example, FGF2 administration caused oligodendrocyte tauopathy in normal white matter, whereas FGF2 overexpression increased generation of oligodendrocyte lineage cells in a model of autoimmune demyelination (6,7). Alternatively, studies in *Fgf2* null mice indicate that endogenous FGF2 inhibits terminal differentiation of OP cells into remyelinating oligodendrocytes (8). In *Fgf2* null mice, oligodendrocyte repopulation of lesions is enhanced following viral demyelination of the spinal cord or cuprizone demyelination of the corpus callosum (CC) (2,9). Furthermore, remyelination is significantly improved in *Fgf2* null mice (2). These studies in *Fgf2* null mice uncover enhanced repair capacity of the endogenous OP population following chronic demyelination.

The current studies test the ability of magnetic resonance diffusion tensor imaging (DTI) to detect the evolution of pathological features associated with chronic demyelination and recovery in *Fgf2* null vs. wild type (wt) mice. Additionally, because FGF2 upregulation promotes neuronal survival in diverse forms of CNS injury (10,11), we evaluated the consequence of FGF2 absence on axon integrity during chronic demyelination. Cuprizone-induced CC demyelination is used to facilitate analysis of remyelination and neuroprotection in *Fgf2* null mice. Cuprizone ingestion in mice induces reproducible and extensive demyelination especially within the caudal CC (12,13), with pathological characteristics of oligodendrocyte loss that are shared with certain MS lesions (14,15). Additionally, MS lesions exhibit 2 main forms of axonopathy. During acute injury in MS the majority of axons develop swellings from disrupted axonal transport followed by recovery during resolution of the inflammatory response (1). Subsequent progression to a chronic disease stage is associated with demyelination, atrophy (i.e. reduced diameter), and slow continuous axon loss (1). The cuprizone model exhibits axonal swellings during the acute stage that resolve after the initial episode of demyelination (13). Following continued cuprizone feeding, axons become chronically demyelinated and atrophic, yet the majority of axons remain viable and recover after a return to normal chow without toxin (13). Importantly, our analysis of regenerative processes is facilitated by this ability to remove the demyelinating agent from the diet.

MATERIALS AND METHODS

Mice and Cuprizone Demyelination

All experimental procedures using mice were approved by the USUHS Institutional Animal Care and Use Committee and/or the Washington University Animal Studies Committee. C57BL/6 mice were purchased from The Jackson Laboratory (Bar Harbor, ME). *Fgf2* null (−/−) and wild type (+/+; wt) mice were derived from breeding pairs provided by Dr. Thomas Doetschman (University of Cincinnati, Cincinnati, OH) (16). All mouse lines were

backcrossed to the C57BL/6 background. Mice were fed ad libitum a diet of 0.2% (w/w) cuprizone (oxalic bis-(cyclohexylidenehydrazide, Sigma-Aldrich, St. Louis, MO), mixed into milled chow pellets (Harlan Teklad, Madison, WI) beginning at 8 weeks of age. Analysis time points during cuprizone treatment and recovery were selected based on previous studies documenting axon and myelin pathology throughout the time course of cuprizone treatment and recovery in C57BL/6 mice and in the *Fgf2* null line (2,9,13,17,18). Mice were examined at 8 weeks of age prior to the start of cuprizone feeding (0 weeks, pre-treatment), during the period of initial oligodendrocyte loss and demyelination at 4 weeks of cuprizone (4 weeks, acute demyelination), after 12 weeks of cuprizone feeding to produce chronic demyelination (12 weeks, chronic demyelination), and after 12 weeks of cuprizone followed by a 6-week recovery period on normal chow (12 weeks cuprizone + 6 weeks off). All mice used were males with the exception of the longitudinal imaging studies in which genders were mixed to facilitate comparisons between littermates because gender should not have an effect in the cuprizone model in C57BL/6 background mice (19).

DTI Analysis of *Fgf2* Mice

Fgf2 wild type and null mice (n = 6 of each genotype) underwent a longitudinal DTI study with scans at selected stages of the disease: pre-treatment (0 weeks), acute demyelination (4 weeks), chronic demyelination (12 weeks) and after recovery on normal chow (12 weeks cuprizone + 6 weeks off), based on our previous studies (2,13,18). An additional cohort of mice was not treated with cuprizone and was studied at 8 weeks of age (age-matched to 0 weeks pre-treatment) and 26 weeks of age (age-matched to 12 weeks cuprizone + 6 weeks off) to assess age-dependent effects. DTI were acquired at each time point using a 4.7 T Oxford Instrument magnet (Oxfordshire, UK) as described (13). Coronal images (11 0.5 mm slices) were acquired throughout the rostral-caudal extent of the CC and were co-registered between scans according to the anatomical position at which the anterior commissure crossed the midline. A multiple-echo spin-echo imaging sequence was used to acquire diffusion-weighted images with the acquisition parameters: TR = 1.5 s, TE = 50 ms, Δ = 25 ms, δ = 8 ms, number of average = 2, number of echo = 3, slice thickness = 0.5 mm, field-of-view = 3 × 3 cm^2, and data matrix = 256 × 256 (zero filled to 512 × 512). Diffusion sensitizing gradients applied along 6 directions: [Gx, Gy, Gz] = [1,1,0], [1,0,1], [0,1,1], [−1,1,0], [0, −1,1], and [1,0, −1]. Two b-values (0 and 0.768 ms/μm^2) were applied. As previously reported (18), the eigen values (λ_1, λ_2, and λ_3) of the diffusion tensor were derived by matrix diagonalization and on a pixel-by-pixel basis, axial ($\lambda_{||}$), and radial diffusivity ($\lambda_{\perp}$), were derived using software written in Matlab (Math Works, Natick, MA). The CC from the midline to under the peak of the cingulum was manually defined as region of interest on the color-coded relative anisotropy maps (Fig. 1E, F) using NIH ImageJ, as in our previous study (13).

Analysis of Myelin and Axon Pathology in *Fgf2* Mice

Fgf2 wild type and null mice (n = 3 mice of each genotype at each time point) were perfused with 2% paraformaldehyde/3% acrolein for processing of alternate sections from the same mouse for electron microscopy and immunohistochemistry (13). Cuprizone-induced abnormalities differ along the rostro-caudal extent of the CC with the most extensive alterations observed in the caudal CC (12,13). Therefore, regions of the CC were examined separately for quantitative analysis corresponding (approximated relative to Bregma) as rostral (+0.25 to +0.75 mm), middle (−0.5 to −1.0 mm) and caudal (−1.5 to −2.0 mm) (13).

Parasagittal sections were processed for electron microscopy, as described (13). Sections were examined in a Philips CM100 transmission electron microscope with 3 micrographs of each region of each mouse acquired by an investigator blinded to the genotype and conditions. Images were imported into MetaMorph (Molecular Devices, Downington, PA)

for quantitative analysis, including axon diameter and myelin thickness. Within each micrograph, all axons within a randomized area were analyzed with at least 100 axons examined per region. Axons with diameters typical of unmyelinated fibers (<0.3 um) were excluded from this analysis to follow more specifically the changes associated with demyelination and remyelination within the myelinated fiber population (13,20). Therefore, the percent myelinated axons for each region was calculated as a percentage of myelinated axons among the total number of axons counted per region, excluding any axons of diameters < 0.3 μm.

Adjacent parasagittal floating 40-μm sections were double-immunostained for total neurofilament (NF200, rabbit polyclonal pan-neurofilament antibody, Chemicon, Billerica, MA) and non-phosphorylated neurofilament (SMI-32, mouse monoclonal IgG; Covance, Princeton, NJ) to evaluate axonal integrity (21). NF200-positive and SMI-32-positive cross-sectional profiles were counted on high magnification images acquired on a Zeiss Pascal confocal microscope with a 63× objective and then imported into Adobe Photoshop 7. Axonal damage was estimated as the percentage of SMI-32-postive profiles among all neurofilament-positive profiles counted (13).

Statistical Analysis

Comparisons for a single mouse genotype or condition across cuprizone time points were examined using one-way ANOVA with a Newman-Keuls post hoc test. Comparisons across 2 genotypes or conditions and multiple cuprizone time points were examined using a two-way ANOVA. Values of 2 genotypes or conditions at a single time point were compared using a *t*-test. Scattergraph data were analyzed by linear regression and comparison of the slopes and intercepts. Double immunofluorescence quantification of the proportion of SMI-32 profiles among those detected with NF200 was assessed using Chi square analysis. A level of 0.05 was used for the overall test of significance. Values are expressed as the mean ± SEM.

RESULTS

DTI Screening of the CC throughout the Cuprizone Time Course of Demyelination through Early Remyelination in *Fgf2* Null and wt Mice

Longitudinal DTI analysis of cohorts of *Fgf2* null and *Fgf2* wt mice was performed to assess overall changes associated with the distinct cuprizone disease stages that we previously characterized histopathologically in C57BL/6 mice (Fig. 1) (13,17,18). Differential analysis of axial and radial diffusivity values focused on the caudal CC in which cuprizone-induced pathology is most extensive (12,13).

Axial diffusivity values reflected a significant effect of cuprizone treatment across time points ($p < 0.0001$) (Fig. 1A). In both *Fgf2* null and wt mice, cuprizone treatment resulted in decreased axial diffusivity values from pre-treatment to 4 weeks of cuprizone (wt, $p < 0.01$; null, $p < 0.001$). These results are consistent with our previous studies in C57BL/6 mice in which reduced axial diffusivity values were observed in regions of axon swellings and varicosities as well as high cell densities from reactive changes in the CC during the onset of cuprizone demyelination (13,18). *Fgf2* genotype did not have an overall effect on axial diffusivity across the time points examined ($p = 0.1368$).

Radial diffusivity values reflected a significant effect of cuprizone treatment across time points ($p < 0.0001$) (Fig. 1B). Importantly, an effect of *Fgf2* genotype was observed across time points ($p < 0.01$). In both *Fgf2* null and wt mice, radial diffusivity values were unchanged from pre-treatment to 4 weeks of cuprizone, but were significantly increased by

12 weeks of cuprizone (wt and null, $p < 0.001$ for each genotype at 12 weeks vs. 4 weeks or pre-cuprizone time points).

After chronic demyelination and 6 weeks recovery, radial diffusivity values remained significantly elevated in *Fgf2* wt mice ($p < 0.001$), whereas in *Fgf2* null mice they were significantly reduced ($p < 0.05$ vs. 12 weeks) and similar to non-treated levels ($p > 0.05$ vs. pre-cuprizone). While *Fgf2* null and wt mice did not exhibit overt differences in the CC on relative anisotropy maps (Fig. 1E, F) during this recovery period, the specific changes detected in the quantitative analysis were evident in the radial diffusivity maps (Fig. 1G, H). The *Fgf2* wt values are similar to those observed in our previous studies in which demyelinated regions of the CC exhibit increased radial diffusivity values that did not recover fully following chronic demyelination even when followed up to 12 weeks after return to normal chow (13, 18). Therefore, the normalization of radial diffusivity in *Fgf2* null mice during the recovery period suggests a significant improvement in remyelination associated with *Fgf2* genotype.

Ultrastructural Analysis of Remyelination

To examine ultrastructural differences for correlations with the DTI changes that may indicate improved remyelination in *Fgf2* null mice, we performed quantitative electron microscopic analysis of the myelination status in the CC (Fig. 2). Following 12 weeks of cuprizone, marked demyelination was noted in mice of both *Fgf2* null and *Fgf2* wt genotypes (Fig. 2B, E), the percentage of myelinated fibers increased during the 6-week recovery period on normal chow, suggesting partial remyelination (Fig. 2C, F). The *Fgf2* null mice had a higher proportion of myelinated axons at 12 weeks of cuprizone ($p < 0.05$) and during the recovery period ($p < 0.05$) as compared to *Fgf2* wt mice (Fig. 2G).

Ultrastructural demonstration of remyelination is based on evidence of reduced myelin thickness relative to axon diameter. For analysis of CC remyelination after cuprizone, the g ratio value (an overall population average value of the ratio of axon diameter to myelinated fiber diameter) is not as sensitive as population distribution analysis using the slope of myelin thickness relative to axon diameter, which displays the distribution of individual fiber changes in myelin thickness relative to axon diameter (13,22). After chronic cuprizone demyelination and a 6-week recovery, both *Fgf2* wt and null mice showed remyelination in a significant proportion of axons when compared with non-treated mice of the same genotype (Fig. 3; comparison of slopes: *Fgf2* wt, $p < 0.05$ for no cuprizone vs. 12 weeks cuprizone + 6 weeks off; *Fgf2* null, $p < 0.05$ for no cuprizone vs. 12 weeks cuprizone + 6 weeks off). After this recovery period, *Fgf2* wt and null mice also show similar myelin thickness relative to axon diameter (Fig. 3C, F; 12 weeks cuprizone + 6 weeks off; $p > 0.05$ for wt vs. null). Importantly, prior to the recovery period there was an *Fgf2* genotype effect (Fig. 3B, E; 12 weeks cuprizone, $p < 0.05$ for *Fgf2* wt vs. *Fgf2* null). Specifically, the myelinated fiber population in *Fgf2* null mice was associated with reduced myelin thickness relative to axon diameter (Fig. 3D, E; *Fgf2* null, $p < 0.05$ for no cuprizone vs. 12 weeks cuprizone). These data indicate remyelination at 12 weeks of cuprizone in *Fgf2* null mice that was not detected in *Fgf2* wt mice (Fig. 3B, E; comparison of slopes; *Fgf2* wt, $p > 0.05$ for no cuprizone vs. 12 weeks cuprizone).

Our ultrastructural data of the percentage of myelinated axons (Fig. 2G) combined with the population analysis of the distribution of myelin thickness relative to axon diameter (Fig. 3) facilitates distinctions between myelinated populations that have not demyelinated and those that have undergone remyelination. Specifically, after 12 weeks of cuprizone the *Fgf2* wt mice had a majority of axons without myelin (Fig. 2G; 15.83 ± 7.6% myelinated) and a slope that is not significantly different from the non-treated *Fgf2* wt population (Fig. 3B). Therefore, in *Fgf2* wt mice the majority of the axon population with myelin after 12 weeks

of cuprizone is comprised of fibers that have myelin thickness similar to those in non-treated mice; presumably these represent normally myelinated axons that did not undergo an episode of demyelination. In contrast, after 12 weeks of cuprizone the *Fgf2* null mice exhibit a higher proportion of axons with myelin (Fig. 2G; 36.9 ± 4.7% myelinated), combined with a slope that is significantly different from the non-treated *Fgf2* null population (Fig. 3E). These combined data indicate that in *Fgf2* null mice a significant proportion of axons with myelin after 12 weeks of cuprizone have undergone remyelination. The potential difference of approximately 20% in the proportion of myelinated axons between *Fgf2* wt and null genotypes after 12 weeks of cuprizone may reflect an increase in remyelinated fibers in the *Fgf2* null mice. This interpretation assumes that approximately 16% of the myelinated axons in the *Fgf2* null mice at 12 weeks may represent fibers that did not demyelinate. This assumption is supported by analysis of *Fgf2* null mice during active demyelination at 4 weeks of cuprizone in which the proportion of myelinated axons was 15.3 ± 6.5%. Therefore, the genotype difference in the proportion of myelinated axons at 12 weeks cannot be due to a lack of demyelination in *Fgf2* null mice. Furthermore, an increase in the proportion of myelinated axons between the 4 to 12 weeks time points ($p < 0.05$, *Fgf2* null, 4 weeks vs. 12 weeks cuprizone) corroborates the myelin thickness data (Fig. 3) and indicates earlier remyelination in *Fgf2* null mice.

Reduced Axonal Damage in Fgf2 Null Mice

We next examined axons in *Fgf2* null and wt mice to characterize the effect of the *Fgf2* null phenotype on axonopathy with chronic demyelination and to evaluate the contribution of axonal pathology to the DTI findings. SMI-32 immunostaining was combined with immunolabeling for NF200, a pan-neurofilament epitope, to detect the total population of axons (Fig. 4A, B). Both *Fgf2* null and wt mice showed an increase in SMI-32 immunostaining in the CC after chronic exposure to cuprizone. The increase of SMI-32 immunolabeling in the *Fgf2* wt mice (Fig. 4C) was similar to that in C57BL/6 mice after chronic cuprizone (13). However, the percentage of SMI-32-positive axons was significantly reduced in *Fgf2* null mice compared to *Fgf2* wt mice (Fig. 4C, D; $p = 0.0059$). This attenuation of neurofilament dephosphorylation was found throughout the CC following analysis of areas within the rostral, middle, and caudal CC (Fig. 4C, D; $p < 0.01$ for rostral and middle, $p < 0.001$ for caudal). Mice of both genotypes show values similar to non-treated levels after the 6-week recovery period on normal chow (Fig. 4C, D). In *Fgf2* null mice, the 12 weeks cuprizone values showed improvement from the acute phase, i.e. at 4 weeks of cuprizone, SMI-32 immunolabeling in *Fgf2* null mice was 22.57 ± 3.15% (middle, $p < 0.05$ vs. 12 weeks) and 31.76 ± 3.34% (caudal, $p < 0.05$ vs. 12 weeks) (Fig. 4D). *Fgf2* null attenuation of neurofilament dephosphorylation at 12 weeks of cuprizone is corroborated by changes in axon diameter because axonal atrophy is indicative of axon damage (Fig. 4E, F). *Fgf2* wt mice showed more marked reduction of axon diameters than *Fgf2* null mice after chronic demyelination (middle and caudal CC, $p < 0.05$ for null vs. wt at 12 weeks cuprizone).

DISCUSSION

The current studies extend our previous work in *Fgf2* null mice by adding 2 independent approaches; both indicate that remyelination is significantly enhanced following chronic demyelination. Importantly, in *Fgf2* null mice we can now detect remyelination at an earlier time point and now reveal a dramatic reduction of chronic axonal abnormalities. Furthermore, we demonstrate the capabilities and limitations of DTI for distinguishing these pathological effects. Specifically, the extent of enhanced remyelination in *Fgf2* null mice is sufficiently robust and generalized to be detectable non-invasively with longitudinal DTI analysis. Electron microscopy confirmed that a greater proportion of demyelinated axons

underwent spontaneous remyelination in *Fgf2* null mice and that remyelination was ongoing during chronic demyelination at 12 weeks of cuprizone ingestion. The ultrastructural studies also demonstrate axonal atrophy during chronic demyelination after 12 weeks of cuprizone in *Fgf2* wt mice that is greatly reduced in *Fgf2* null mice. The effect of FGF2 absence in protection from chronic axonopathy was further supported by immunohistochemical studies showing reduced neurofilament dephosphorylation during chronic demyelination in *Fgf2* null mice. However, DTI analysis did not detect this attenuation of chronic axonopathy in *Fgf2* null mice.

The neuroprotective effects in *Fgf2* null mice are an important clue to understanding how to prevent early stage axon damage from progressing to discontinuity and permanent neurological deficits in demyelinating diseases. FGF2 can be synthesized by reactive astrocytes and by activated microglia and macrophages in demyelinated lesions (23). Diverse cellular components in the lesion environment including axons, astrocytes, microglia, as well as oligodendrocyte lineage cells can express multiple FGF receptor (FGFR) isoforms that may respond differentially to FGF2 (24,25). Given this complexity, the improved axon integrity observed in the absence of FGF2 may result from direct effects on axons or indirect effects through multiple cell types. For example, FGF2 has been reported to act through FGF receptor 1 (FGFR1) on astrocytes to induce scarring characteristics (24), which could drive the lesion environment to be less favorable for axon homeostasis. Oligodendrocytes may have trophic effects on axons and remyelination may protect denuded axons from further insult (1,26), processes that may also contribute indirectly to the axon protection observed in *Fgf2* null mice. In the peripheral nervous system, increased axon size and myelination were observed in *Fgf2* null mice after sciatic nerve injury (27), indicating potential common beneficial effects of FGF2 removal for axons in both the central and peripheral nervous systems. Combining these findings with those of beneficial effects of FGF2 on neuronal survival (10,11), we propose a model of differential effects of FGF2 upregulation following injury in which FGF2 directly promotes neuronal, i.e. cell body, survival while indirectly impairing axonal recovery. In white matter tracts, FGF2 may act indirectly to induce an astroglial scarring phenotype and/or inhibit OP differentiation and remyelination, which may create conditions that leave axons vulnerable to further damage and do not sufficiently support axon health or recovery.

Electron microscopy provides a more detailed characterization of remyelination in *Fgf2* null vs. wt mice than was possible with our previous immunohistochemical analysis of myelin associated glycoprotein (MOG) (2). MOG immunostaining of the CC in cuprizone-treated mice has advantages for analyzing large lesion areas and correlates well with Luxol fast blue myelin staining (28). However, both immunohistochemistry for MOG and LFB staining are less sensitive than electron microscopy for detecting remyelination (28). Consistent with this difference in technique sensitivity, the ongoing remyelination in *Fgf2* null mice was detected at 12 weeks by electron microscopy but not by quantification of MOG immunostaining (2).

Whether FGF2 limits remyelination by acting directly on oligodendrocyte lineage cells or indirectly through other cells in the lesion environment is not yet clear. Retroviral lineage tracing, to monitor differentiation of endogenous cycling cells during the course of cuprizone demyelination and remyelination, demonstrated increased differentiation of OP cells into oligodendrocytes in *Fgf2* null mice, indicating that FGF2 in lesions may limit remyelination by inhibiting OP differentiation (8). RNA interference studies of cultured OP cells show that FGF2 can act through FGFR1 to regulate OP differentiation into oligodendrocytes (29). In the context of the demyelinated lesion environment, FGF2 may also activate FGFR1 on astrocytes to induce glial scarring, thereby indirectly inhibiting remyelination.

This is the first demonstration of the use of DTI to detect changes associated with a genetic manipulation that improved recovery from demyelinating disease. The work complements a similar study that demonstrated DTI detection of improved remyelination pharmacologically stimulated by thyroid hormone treatment during a recovery period following chronic demyelination (30). These studies provide proof-of-principle for non-invasive longitudinal DTI assessments that can be applied to help evaluate interventions for promoting remyelination in translational studies. Longitudinal functional and imaging assessments provide critical comparisons across disease stages to assess the extent of disease severity and the subsequent recovery achieved. Our earlier studies in C57BL/6 mice with scans every other week throughout the cuprizone time course identified 4 weeks of cuprizone as the peak of reduced axial diffusivity while radial diffusivities were elevated from 6 to 12 weeks of cuprizone and remained elevated during the recovery period (17,18). The decrease of axial diffusivity at 4 weeks of cuprizone correlates with early stage axonal damage, axon swelling and neurofilament dephosphorylation, along with a high density of CD11b-immunolabeled microglia/macrophage cells in the CC (13). During the chronic demyelination stage, axonal swellings resolve to relatively uniform axonal profiles, although axonopathy is still indicated by axon diameter reduction (13). DTI axial diffusivity values during chronic demyelination were not significantly different from controls, possibly reflecting dissipation of microglia/macrophage populations (13), or increased extracellular volume masking axonal damage effects of decreasing axial diffusivity. Accordingly, the reduction of chronic stage axonopathy in *Fgf2* null mice was not detected by DTI axial diffusivity. The DTI detected signal reflects the volume average effect of the environment on the image voxel in the anatomical region of interest quantified. Because the CC contains both myelinated and unmyelinated axons, potential changes in unmyelinated axons during chronic demyelination might also be undetected with the current techniques. In contrast, the periods of elevated radial diffusivity generally correspond with histological and ultrastructural evidence of demyelination in the CC (13). Importantly, we distinguished a significant normalization of radial diffusivity values after removal of cuprizone from the diet in the *Fgf2* null mice vs. the wt mice. This difference of radial diffusivity during the recovery period correlated with ultrastructural evidence of significantly improved remyelination in *Fgf2* null mice.

These studies support the expectation that recovery from chronic demyelination may be enhanced through therapeutic strategies that reduce signals inhibiting OP differentiation. FGF2 signaling is an effective component limiting remyelination of chronically demyelinated lesions. The pleiotrophic effects of FGF2 create an unfavorable profile for therapeutic development so that further studies are needed to characterize the relevant FGFR components and more specific therapeutic targets. The dramatic neuroprotective effect observed with genetic removal of FGF2 requires further study to identify the specific molecular mechanisms that may be involved and potentially exploited to prevent accrual of axonal damage and loss during chronic demyelination. DTI will be an important tool for longitudinal monitoring and screening of reagents to promote remyelination but will require complementary imaging techniques to evaluate chronic axonopathy.

Acknowledgments

This work was supported by the National Institutes of Health Grants NS47592 (SKS), NS54194 (SKS) and NS39293 (RCA) and National Multiple Sclerosis Society Grants RG3515 (RCA), RG 3670A3/2 (SKS). We appreciate the assistance of Mr. Chris Doe, Ms. Lauren Harris, and Dr. Dennis McDaniel for the electron microscopy and confocal analysis.

We appreciate the assistance of Mr. Chris Doe, Ms. Lauren Harris, and Dr. Dennis McDaniel for the electron microscopy and confocal analysis.

References

1. Trapp BD, Stys PK. Virtual hypoxia and chronic necrosis of demyelinated axons in multiple sclerosis. Lancet Neurol. 2009; 8:280–91. [PubMed: 19233038]
2. Armstrong RC, Le TQ, Flint NC, et al. Endogenous cell repair of chronic demyelination. J Neuropathol Exp Neurol. 2006; 65:245–56. [PubMed: 16651886]
3. John GR, Shankar SL, Shafit-Zagardo B, et al. Multiple sclerosis: re-expression of a developmental pathway that restricts oligodendrocyte maturation. Nat Med. 2002; 8:1115–21. [PubMed: 12357247]
4. Mi S, Miller RH, Tang W, et al. Promotion of central nervous system remyelination by induced differentiation of oligodendrocyte precursor cells. Ann Neurol. 2009; 65:304–15. [PubMed: 19334062]
5. Back SA, Tuohy TM, Chen H, et al. Hyaluronan accumulates in demyelinated lesions and inhibits oligodendrocyte progenitor maturation. Nat Med. 2005; 11:966–72. [PubMed: 16086023]
6. Ruffini F, Furlan R, Poliani PL, et al. Fibroblast growth factor-II gene therapy reverts the clinical course and the pathological signs of chronic experimental autoimmune encephalomyelitis in C57BL/6 mice. Gene Ther. 2001; 8:1207–13. [PubMed: 11509953]
7. Butt AM, Dinsdale J. Fibroblast growth factor 2 mediated disruption of myelin-forming oligodendrocytes in vivo is associated with increased tau immunoreactivity. Neurosci Lett. 2005; 375:28–32. [PubMed: 15664117]
8. Murtie JC, Zhou YX, Le TQ, et al. PDGF and FGF2 pathways regulate distinct oligodendrocyte lineage responses in experimental demyelination with spontaneous remyelination. Neurobiol Dis. 2005; 19:171–82. [PubMed: 15837572]
9. Armstrong RC, Le TQ, Frost EE, et al. Absence of fibroblast growth factor 2 promotes oligodendroglial repopulation of demyelinated white matter. J Neurosci. 2002; 22:8574–85. [PubMed: 12351731]
10. Teng YD, Mocchetti I, Taveira-DaSilva AM, et al. Basic fibroblast growth factor increases long-term survival of spinal motor neurons and improves respiratory function after experimental spinal cord injury. J Neurosci. 1999; 19:7037–47. [PubMed: 10436058]
11. Alzheimer C, Werner S. Fibroblast growth factors and neuroprotection. Adv Exp Med Biol. 2002; 513:335–51. [PubMed: 12575827]
12. Wu QZ, Yang Q, Cate HS, et al. MRI identification of the rostral-caudal pattern of pathology within the corpus callosum in the cuprizone mouse model. J Magn Reson Imaging. 2008; 27:446–53. [PubMed: 17968901]
13. Xie M, Tobin JE, Budde MD, et al. Rostro-caudal analysis of corpus callosum demyelination and axon damage across disease stages refines diffusion tensor imaging correlation with pathological features. J Neuropathol Exp Neurol. 2010; 69:704–16. [PubMed: 20535036]
14. Lucchinetti C, Bruck W, Parisi J, et al. A quantitative analysis of oligodendrocytes in multiple sclerosis lesions. A study of 113 cases. Brain. 1999; 122:2279–95. [PubMed: 10581222]
15. Liu L, Belkadi A, Darnall L, et al. CXCR2-positive neutrophils are essential for cuprizone-induced demyelination: relevance to multiple sclerosis. Nature Neuroscience. 2010; 13:319–26.
16. Zhou M, Sutliff RL, Paul RJ, et al. Fibroblast growth factor 2 control of vascular tone. Nat Med. 1998; 4:201–7. [PubMed: 9461194]
17. Song SK, Yoshino J, Le TQ, et al. Demyelination increases radial diffusivity in corpus callosum of mouse brain. NeuroImage. 2005; 26:132–40. [PubMed: 15862213]
18. Sun SW, Liang HF, Trinkaus K, et al. Noninvasive detection of cuprizone induced axonal damage and demyelination in the mouse corpus callosum. Magn Reson Med. 2006; 55:302–8. [PubMed: 16408263]
19. Taylor LC, Gilmore W, Ting JP, et al. Cuprizone induces similar demyelination in male and female C57BL/6 mice and results in disruption of the estrous cycle. J Neurosci Res. 2010; 88:391–402. [PubMed: 19746424]
20. Mason JL, Langaman C, Morell P, et al. Episodic demyelination and subsequent remyelination within the murine central nervous system: changes in axonal calibre. Neuropathol Appl Neurobiol. 2001; 27:50–8. [PubMed: 11299002]

21. Trapp BD, Peterson J, Ransohoff RM, et al. Axonal transection in the lesions of multiple sclerosis. N Engl J Med. 1998; 338:278–85. [PubMed: 9445407]
22. Stidworthy MF, Genoud S, Suter U, et al. Quantifying the early stages of remyelination following cuprizone-induced demyelination. Brain Pathol. 2003; 13:329–39. [PubMed: 12946022]
23. Messersmith DJ, Murtie JC, Le TQ, et al. Fibroblast growth factor 2 (FGF2) and FGF receptor expression in an experimental demyelinating disease with extensive remyelination. J Neurosci Res. 2000; 62:241–56. [PubMed: 11020217]
24. Smith C, Berry M, Clarke WE, et al. Differential expression of fibroblast growth factor-2 and fibroblast growth factor receptor 1 in a scarring and nonscarring model of CNS injury in rat. Eur J Neurosci. 2001; 13:443–56. [PubMed: 11168551]
25. Fortin D, Rom E, Sun H, et al. Distinct fibroblast growth factor(FGF)/FGF receptor signaling pairs initiate diverse cellular responses in the oligodendrocyte lineage. J Neurosci. 2005; 25:7470–9. [PubMed: 16093398]
26. Bruce CC, Zhao C, Franklin RJ. Remyelination - An effective means of neuroprotection. Horm Behav. 2009; 57:56–62. [PubMed: 19538961]
27. Jungnickel J, Haastert K, Grzybek M, et al. Mice lacking basic fibroblast growth factor showed faster sensory recovery. Exp Neurol. 2010; 223:166–72. [PubMed: 19520074]
28. Lindner M, Heine S, Haastert K, et al. Sequential myelin protein expression during remyelination reveals fast and efficient repair after central nervous system demyelination. Neuropathol Appl Neurobiol. 2008; 34:105–14. [PubMed: 17961136]
29. Zhou YX, Flint NC, Murtie JC, et al. Retroviral lineage analysis of fibroblast growth factor receptor signaling in FGF2 inhibition of oligodendrocyte progenitor differentiation. Glia. 2006; 54:578–90. [PubMed: 16921523]
30. Harsan LA, Steibel J, Zaremba A, et al. Recovery from chronic demyelination by thyroid hormone therapy: myelinogenesis induction and assessment by diffusion tensor magnetic resonance imaging. J Neurosci. 2008; 28:14189–201. [PubMed: 19109501]

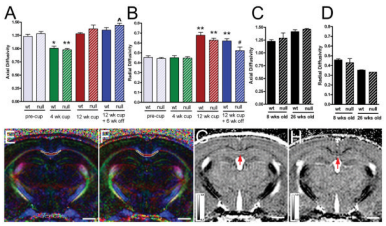

Figure 1.

Diffusion tensor imagine (DTI) in the corpus callosum (CC) of *Fgf2* null and wild type (wt) mice throughout the course of cuprizone (cup) treatment and recovery. (**A, B**) Quantification of axial (**A**) and radial (**B**) diffusivity in the caudal CC. Cohorts of *Fgf2* wt and *Fgf2* null mice (n = 6 each) underwent a longitudinal DTI study comprised of pre-treatment (pre-cup, 8 weeks of age), the onset of demyelination (4 weeks of cup), during chronic demyelination (12 weeks), and after a recovery period (12 weeks of cup followed by 6 weeks on normal chow without cup). Axial diffusivity values (**A**) were not different between *Fgf2* null and wt mice across the time points examined ($p > 0.05$); both exhibited a significant decrease from pre-treatment values only at the 4-week time point (wt, $p < 0.01$, null $p < 0.001$). Radial diffusivity values (**B**) did not change from pre-treatment values until they increased significantly between 4 and 12 weeks of cup in both *Fgf2* genotypes (both wt and null, $p < 0.001$ at 12 weeks, compared within genotype with 4 weeks or pre-cup values). In *Fgf2* wt mice, radial diffusivity values after the 6-week recovery period still remained significantly increased from the pre-treatment time point ($p < 0.001$). *Fgf2* null mice exhibited a significant decrease (i.e. normalization) of radial diffusivity values after the 6-week recovery period ($p > 0.05$ vs. pre-cup; $p < 0.05$ vs. 12 weeks). (**C, D**) Quantification of axial (**C**) and radial (**D**) diffusivity in the caudal CC of a separate cohort of mice without cup treatment with longitudinal evaluation for age-related changes at 8 weeks (equivalent to pre-cup) and 26 weeks (equivalent to 12 weeks cup + 6 weeks off). *Fgf2* wt (n = 4) and null (n = 2) values appear similar at each time point; thus, although an age effect is present even in non-treated wt mice (8 vs. 26 weeks *Fgf2* wt; $p = 0.0084$ axial; $p = 0.002$ radial), age cannot account for the difference in radial diffusivity between *Fgf2* wt and null mice during recovery from cup. (**E, F**) Color-coded relative anisotropy (RA) maps show the region of interest (ROI) analyzed in the caudal CC. The color of the RA map reflects the fiber orientation (red, medial-lateral; green, superior-inferior; blue, anterior-posterior) within white matter tracts. ROI (white outlined area) was defined manually in the caudal CC from the midline to under the peak of the cingulum. Examples shown are from *Fgf2* wt (**E**) and *Fgf2* null mice (**F**) after 12 weeks of cup followed by a 6-week recovery period on normal chow. (**G, H**) Representative radial diffusivity maps from *Fgf2* wt (**G**) and *Fgf2* null (**H**) mice after 12 weeks of cuprizone followed by a 6-week recovery period on normal chow. Normalization in *Fgf2* null CC is consistent with more extensive remyelination. The red arrows point to areas of the CC showing differences in radial diffusivity. Scale bar = 1 mm. Comparisons with pre-cup shown as ^$p < 0.05$, *$p < 0.01$, **$p < 0.001$ and relative to 12 weeks cup as # $p < 0.05$.

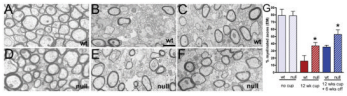

Figure 2.

Ultrastructural analysis of myelination in Fgf2 null and wt mice. (**A–F**) Electron micrographs of corpus callosum (CC) in *Fgf2* wild type (wt) (**A–C**) and *Fgf2* null (**D–F**) mice illustrate normal myelination in non-treated (26 weeks) controls (**A, D**), demyelination after 12 weeks of cuprizone (cup) (**B, E**), and remyelination after 12 weeks of cup and 6 weeks on normal chow (**C, F**). (**G**) The percent of myelinated axons quantified in caudal region of the CC. *Fgf2* null mice have a higher proportion of myelinated axons at 12 weeks of cup and during the 6-week recovery period compared to *Fgf2* wt mice ($p < 0.05$ between genotypes across all time points). *$p < 0.05$ for comparisons of genotypes at each time point.

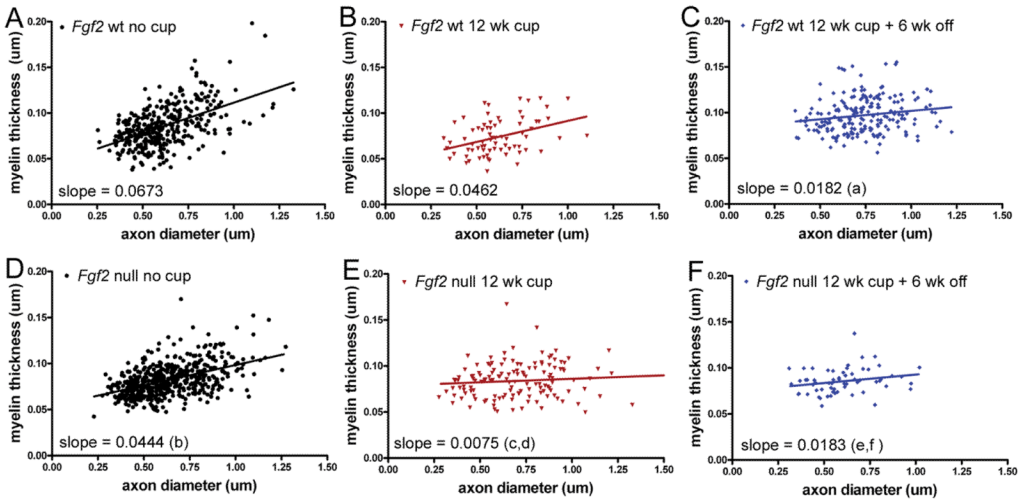

Figure 3.

Relationship of myelin thickness to axon diameter in Fgf2 null and wild type (wt) mice. Scatter plots of individual axons in the caudal corpus callosum for *Fgf2* wt (**A–C**) and *Fgf2* null (**D–F**) mice in non-treated (26 weeks) controls (**A, D**), demyelination after 12 weeks of cuprizone (cup) (**B, E**), and after 12 weeks of cup and 6 weeks on normal chow (**C, F**). (**A–C**) In *Fgf2* wt mice, thinner myelin relative to axon diameter (indicative of remyelination) is demonstrated by the significantly reduced slope observed during the recovery period (**a**, *Fgf2* wt, $p < 0.05$, no cup vs. 12 weeks cup + 6 weeks off). (**D–F**) In comparison with *Fgf2* wt mice, *Fgf2* null mice have thinner myelin prior to cup treatment (**b**, no cup $p < 0.05$, wt vs. null). *Fgf2* null mice exhibit significantly reduced slopes from non-treated *Fgf2* null mice after both 12 weeks of cup (**c**, $p < 0.05$, no cup vs. 12 weeks cup) and during the recovery period (**e**, $p < 0.05$, no cup vs. 12 weeks cup + 6 weeks off), indicating significant remyelination at the 12-week time point and continuing during the recovery period. Importantly, the slopes are also significantly different for the *Fgf2* null mice vs. *Fgf2* wt mice at 12 weeks of cup (**d**, wt vs. null, $p < 0.05$ at 12 weeks cup), indicating earlier remyelination in *Fgf2* null mice than in wt mice. The slopes are not different for *Fgf2* null vs. wt mice after the recovery period (**f**, wt vs. null, $p > 0.05$), indicating that the myelin thickness of remyelinated fibers is similar between genotypes even though *Fgf2* null mice started with thinner myelin prior to cup treatment (**b**).

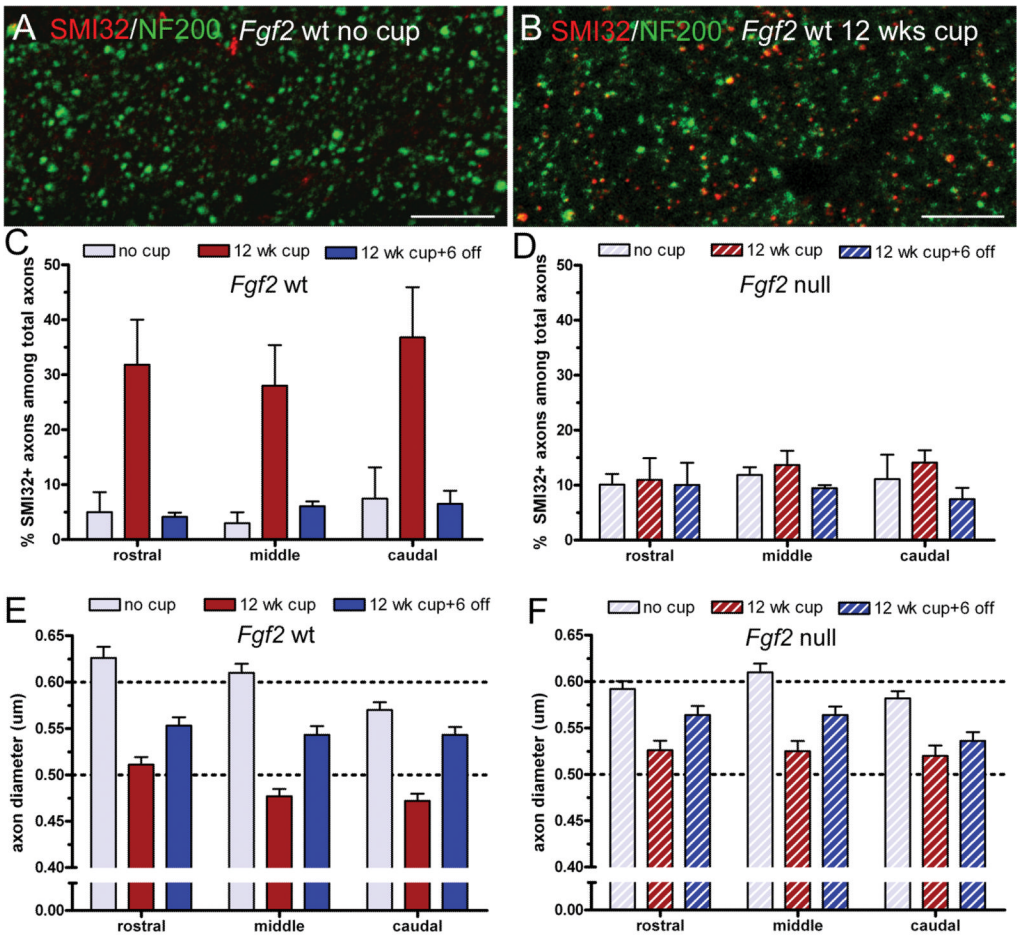

Figure 4.

Axon damage in Fgf2 null and wild type (wt) mice. (**A, B**) Representative confocal microscopy images of double immunolabeling with NF200 (green; pan-neurofilament marker), and SMI-32 (red; non-phosphorylated neurofilament epitope), in the caudal corpus callosum (CC) of *Fgf2* wt mice without cuprizone (cup) (**A**) and after 12 weeks of cup to illustrate the increase of SMI-32 immunolabeling (**B**). Scale bar = 20 μm. (**C, D**) Quantification of the proportion of SMI-32-labeled axons in the rostral, middle and caudal CC of *Fgf2* wt (**C**) and null (**D**) mice that are non-treated (26 weeks) controls (no cup), fed cup for 12 weeks (12 weeks cup), or fed cup for 12 weeks followed by 6 weeks on normal chow (12 weeks cup + 6 off). After 12 weeks of cup, significantly fewer axons are SMI-32-positive in *Fgf2* null mice (**D**) vs. *Fgf2* wt mice (**C**) (2-way ANOVA $p = 0.0059$, rostral $p < 0.01$, middle $p < 0.01$, caudal $p < 0.001$). (**E, F**) Quantification of axon diameter in electron micrographs from *Fgf2* wt (**E**) and null (**F**) mice. (Representative ultrastructural images are shown in Fig. 2). After 12 weeks of cup, mean axon diameters are significantly reduced in *Fgf2* wt mice; this atrophy is attenuated in *Fgf2* null mice (**F**) (middle $p < 0.05$, caudal $p < 0.05$).